creative commons
COMMONS DEED

저작자표시-비영리-변경금지 2.0 대한민국

이용자는 아래의 조건을 따르는 경우에 한하여 자유롭게

- 이 저작물을 복제, 배포, 전송, 전시, 공연 및 방송할 수 있습니다.

다음과 같은 조건을 따라야 합니다:

저작자표시. 귀하는 원저작자를 표시하여야 합니다.

비영리. 귀하는 이 저작물을 영리 목적으로 이용할 수 없습니다.

변경금지. 귀하는 이 저작물을 개작, 변형 또는 가공할 수 없습니다.

- 귀하는, 이 저작물의 재이용이나 배포의 경우, 이 저작물에 적용된 이용허락조건을 명확하게 나타내어야 합니다.
- 저작권자로부터 별도의 허가를 받으면 이러한 조건들은 적용되지 않습니다.

저작권법에 따른 이용자의 권리는 위의 내용에 의하여 영향을 받지 않습니다.

이것은 이용허락규약(Legal Code)을 이해하기 쉽게 요약한 것입니다.

Disclaimer

dCollection

공학석사 학위논문

Bioglass-incorporated gelatin based cryogel for osteogenic commitment of mesenchymal stem cell

바이오글라스 기반 생체재료를 통한 줄기세포의 골형성 유발

2018.02

서울대학교 대학원

화학생물공학부

권 송

Abstract

Bioglass-incorporated gelatin based cryogel for osteogenic commitment of mesenchymal stem cell

Song Kwon
School of Chemical and Biological Engineering
The Graduate School
Seoul National University

Bioglass is widely used in medical field as an excellent biomaterial due to its osteo-inducing effect and biocompatibility. However, due to its brittleness, bioglass alone is not an ideal material for implantation. Characteristics of ideal scaffold using in bone tissue engineering are biocompatibility, high pore size, biodegradability, and mechanical property. Methacrylated gelatin (GelMA), which is a modified gelatin form, retains cell adhesion site, which is a well-suited material for cryogel fabrication. Herein, we fabricated bioglass-incorporated GelMA cryogel for testing osteogenic effect. We demonstrated that as doses of bioglass concentration in scaffolds increases, osteogenic effect on mesenchymal cells increases in

in vitro testing. Furthermore, *in vivo* testing supports that bioglass incorporated GelMA cryogel induces stronger osteogenic differentiation on mesenchymal stem cells than the control group, GelMA cryogel.

In this paper, the enhancement of osteogenic effect using bioglass embedded GelMA scaffold will be presented.

Keywords: Methacrylated gelatin, bioglass, hydrogel, bone tissue engineering

Student Number : 2015-22824

CONTENTS

LISTS OF FIGURES AND TABLES

CHAPTER 1.

1.1 Bone tissue engineering

Bone regeneration following surgical removal of bone, injuries arising from sports, trauma, and disease is a challenging obstacle in clinical treatment which can result in impairing the quality of life for the patients. To augment bone defect, autografts and allografts were widely used to treat bone defects [1, 2]. Clinically, Masquelet technique [3] and Reamer-Irrigator-Aspirator system [4], either independently or in combination [5] are frequently used procedures for effective bone regeneration. Even though these procedures use bone grafts which possess necessary attributes such as molecular cues, osteogenic cells and niche for bone regrowth, but it still requires surgical procedures for retrieving the bone graft with its associated disadvantages [6]. Using allografts which could compensate morbidity, but there is a possibility of transferring disease from donors [1, 7]. In this aspect, synthetic biomaterial-based scaffolds that can be designed to emulate native bone structure are one of viable options for the clinicians [8-11]. Among them, cryogel based scaffolds are being explored by the researchers for the bone regeneration. Designing an effective biomaterial-based scaffold requires the system to be biocompatible, biodegradable, adequate

mechanical strength with high inter-connected pore and optimal pore size [11, 12].

1.2 Methacrylated gelatin hydrogel

Synthetic polymers such as polyacrylamide (PAAM) [13], poly(vinyl alcohol) (PVA) [14], and alginate [15] were used as a cryogel material. Synthetic polymers can control degradation rate, yet they are mostly bio-inert and lacks cell binding moieties. Studies for developing new scaffolds were mainly focused on biological moieties, and various types of scaffolds were fabricated from naturally derived polymers [16-19]. Among various candidates, gelatin which is derived from collagen has various biological characteristic including Arg–Gly–Asp (RGD) sequence which help in cell adhesion, cell migration, differentiation and migration, extracellular matrix(ECM) similar to bone and matrix metalloprotein (MMP) degradation sites [20, 21]. Unmodified gelatin hydrogel lacks mechanical integrity. Therefore, many strategies were employed to prepare mechanically stable hydrogel. Chemical moieties are added to increase mechanical stiffness which includes, furan [22, 23], methacrylate [24] and so forth. These moieties were added for preparing photo crosslinked gelatin hydrogels [25, 26]. Methacrylation of gelatin (gelMA) has been widely studied for photo-

polymeriable hydrogel. Furthermore, the mechanical property and porosity of gelMA-based scaffold can be tuned via varying the degree of methacrylic-group substitution during the gelMA synthesis [20]. Nonetheless, using only methacrylated gelatin does not sufficiently induce stem cells to osteogenically differentiate.

1.3 Bioglass

Bioglass (SiO_2-CaO-P_2O_5) like other calcium phosphate attracted attention in bone tissue engineering due to its osteoinductive, biocompatibility and ability to form strong bond with bone and soft tissues [29, 30]. It is widely known that silicon, and calcium ions are more critical which can affect the cell differentiation and can regulate the cell cycle [31-33]. Bioglass can form a bond with host tissue via formation of hydroxyapatite on its surface through surface chemistry in physiochemical condition [11, 34]. However, due to its brittleness, bioglass alone cannot be used as implants, it can be mixed with the biopolymers to result in composite scaffolds which possess bioactivity and plasticity [35].

CHAPTER 2.

2.1 Introduction

In this study, we aimed to investigate the bioactivity of bioglass on bone regeneration via fabricating bioglass-embedded methacrylated gelatin based cryogel. We evaluated the mechanical strength, internal structure, cytotoxicity, osteogenic differentiation and further carried out bone regeneration study in mouse cranial defect model. Herein, we demonstrated that bioglass-embedded methacrylated gelatin based cryogel induced osteogenic differentiation of human tonsil-derived stem cells (hTMSCs) via observing induced osteo-gene level, calcium deposition, and enhanced bone regeneration *in vivo* study.

2.2 Materials and methods

Synthesis of methacrylated gelatin

Methacrylated gelatin (gelMA) was synthesized by first dissolving type A porcine skin gelatin (Sigma Aldrich) into Dulbecco's phosphate buffer saline (DPBS; Sigma Aldrich) at 60 °C for 1 hour to reach 10% (w/v) uniform solution. 8% (v/v) of methacrylic anhydride (Sigma-Aldrich) was

then added to 10% (w/v) gelatin solution at a rate of 0.5 mL/min under stirred condition and reacted for 3 hours at 50 °C. Following solution was 5x-diluted with warm Dulbecco's phosphate buffer saline (Gibco) and dialyzed using 12-14 kDa cutoff dialysis tube (Sigma-Aldrich) in water for 7 days at 40°C. The dialyzed solution was placed at -80°C for a day and lyophilized for another 7 days. After lyophilization, white foam-type sponge was collected and stored at -20 °C for further use.

Preparation of bioglass

7.639 g of calcium nitrate (Sigma Aldrich) was added to 120 mL of deionized water. 9.826 mL of TEOS (Sigma Aldrich) was diluted in 60 mL of ethanol and added to calcium nitrate solution. Citric acid was then prepared to adjust pH of the solution to between 1 and 2. Under vigorous stirring, the prepared solution was dropped at a rate of 0.5mL/sec into ammoniated deionized water, which was prepared by dissolving 1.078g of ammonium dibasic phosphate (Sigma Aldrich) in 1500 mL of deionized water and pH of the ammoniated deionized water was retained around 11 using ammonium hydroxide solution. The solution was kept stirring for 48 hours and aged for another 24 hours. The following solution and its precipitate were separated by centrifuging at 600 xg, and precipitate was

washed three times with deionized water. The precipitate was mixed with 200 mL of 2 % PEG (Sigma Aldrich) solution and suspended for 30 minutes at room temperature. The precipitate was stored at -80°C and was lyophilized for 5 days. The precipitate was sintered at 700°C in a furnace for 3 hours in heating rate of 200 °C/hour. The bioglass was stored at room temperature for further use.

Fabrication of gelMA-bioglass cryogel

10 % (w/v) lyophilized gelMA was fully dissolved in DPBS (Sigma-Aldrich) at 60°C, and 0.5 wt %, 1.5 wt %, 2.5 wt % of bioglass were added to gelMA dissolved solution. For each solution, 0.5 % (w/v) of ammonium persulfate (Sigma Aldrich) and 0.25 % (v/v) of N, N, N', N'-tetramethylethylenediamine (Sigma Aldrich) were added to initiate polymerization. The solutions then were pipetted to 200 µl mold and placed at -20 °C for 24 hours to slow down polymerization reaction while maximize ice crystal fragment for bigger pores. After gelation, ice fragments were removed by lyophilization and cryogels were obtained. Cryogels were stored at -80 °C for further use.

Swelling ratio and mechanical property of scaffold

Swelling ratio test was preformed to investigate water retention of cryogels according to bioglass concentration. For swelling tests, dry weights of each cryogel were measured and transferred to DPBS (Sigma Aldrich) for a day to swell. After 24 hours, cryogels in DPBS were collected and swelling weights of each cryogels were measured. The average swelling ratios of cryogels were calculated based on following equation:

Swelling ratio = $\frac{W_s}{W_d}$

W_s is the swell weight of cryogels and W_d is dried weight of cryogels.

Cryogels were swollen in DPBS for 24 hours, and tested for Young's modulus using the instron. The dataset was then analyzed using the equation:

Young's modulus = $\frac{\sigma}{\varepsilon}$

σ represents stress and ε represents strains.

Degradation by collagenase

Degradation rates of 10% (w/v) gelMA cryogels, gelMA: 0.5 (w/v) bioglass cryogels, gelMA: 1.5 bioglass cryogels, and gelMA: 2.5 bioglass cryogels were measured by placing them in 1 unit/mL of collagen II solution (Worthington Biochemical). Samples were incubated in 37 °C, and old collagenase solutions were replaced with new collagenase solutions

everyday. Cryogels were removed from the collagenase solutions, and water on the surface of cryogels was removed before swollen weights of cryogel were measured at a time point.

Ion release analysis

Bioglass powder was autoclaved before measuring ion release level to remove any contaminants. Then, gelMA cryogels, gelMA-0.5% bioglass cryogels, gelMA-1.5% bioglass cryogels, and gelMA-2.5% bioglass cryogels were fabricated (n = 3), and placed at 24 well plates and filled with 1 mL of simulated body fluid solution. The solution was collected at day 1, 3, 5, and 7, and centrifuged at 4000 rpm for 30 minutes. Solutions then were filtered using 200 nm pore sizes of syringe membrane (Acrodisc®) after samples were collected. Ion release rate of Ca, Si, and P ions were the measured with inductively coupled plasma atomic emission spectrometer (PerkinElmer). The following protocol was used to measure ion release rates of bioglass-embedded cryogels in deionized water.

Scanning Electron Microscopy

Internal structures of cryogels with different concentration of bioglass were observed via scanning electron microscopy (FE-SEM; JSM-

6701F, JEOL). cross-sections of cryogels were fixed on mounts and coated with platinum at 20 mA for 100 seconds. Then, internal structures were analyzed by Field emission electron microscopy (FE-SEM; JSM-6701F, JEOL)

Cell cultures

Human tonsil-derived mesenchymal stem cells (hTMSCs) were isolated from tonsillar tissue after provided from Ewha Womans University Medical Center (Seoul, Korea) with prior consent. For proliferation, hTMSCs were cultured in general medium, which the composition of the solution was 10% fetal bovine serum (Biowest), 1 % L- glutamine (Sigma), 1 % penicillin/streptomycin (Gibco), and 1 % antibiotic-antimycotic (Gibco) in Dulbecco's modified Eagle's medium (Gibco). For differentiation, hTMSCs were cultured in osteogenic medium, the solution of 10mM glycerol-2-phosphate (Sigma), 1% of 2-Phospho-$_{L}$-ascorbic acid (Sigma), 1 % dexamethasone (Sigma), 10% fetal bovine serum (Biowest), and 1% penicillin/streptomycin (Gibco) in Dulbecco's modified Eagle's medium. The culture medium was changed every other day.

Cell viability

Cell viability was observed via Live/Dead viability kit (Invitrogen™). 5 x 10^5 cells of hTMSCs were seeded per cryogels and were incubated for 24 hours. After 24 hours, cryogels were washed with DPBS for three times, and 1mL of DPBS including 2 µl calcein AM and 1 µl ethidium homodimer-1 was added to each cryogels. Cryogels were incubated for 30 minutes and was measured by LSM 720 confocal microscope.

Real Time-PCR

RNAs were extracted from the cell-laden gelMA and gelMA-bioglass cryogel (n = 3) with Trizol (Life Technology). The concentration of RNA, which was extracted was measured by NanoDrop spectrometer (ND-2000; NanoDrop Technologies), and reverse-transcribed into cDNA using TOPscript™ Reverse Transcriptase Kit (Enzynomics). Real time-PCR was performed using ABI StepOnePlus™ real-time PCR system (Applied Biosystems). cDNA samples were analyzed for relative gene expression of GAPDH, OCN, Collagen I, and Runx2 when GAPDH was used as a house-keeping gene. Relative gene expressions of interests were calculated using $-2^{\Delta\Delta Ct}$ method. Primer sequences that were used in RT-PCR were: GAPDH (Forward: 5'-CGC TCT CTG CTC CTC CTG TT-3', Reverse: 5'-CCA TGG

TGT CTG AGC GAT GT-3'), OCN (Forward: 5'-GCC TTT GTG TCC AAG C-3', Reverse: 5'-GGA CCC CAC ATC CAT AG-3'), Collagen I (Forward: 5'-GTC ACC CAC CGA CCA AGA AAC C-3', Reverse: 5'-AAG TCC AGG CTG TCC AGG GAT G-3'), Runx2 (Forward: 5'-ACT GGG CCC TTT TTC AGA-3', Reverse: 5'-GCG GAA GCA TTC TGG AA-3').

Alizarin Red Staining

After 21 days of differentiation, cells were washed with DPBS twice, and were fixed using 4% paraformaldehyde for 15 minutes at room temperature. Fixed cells were stained with 2 % alizarin red staining solution for 20 minutes, and washed three times with distilled water for 5 minutes each.

Calvarial defect surgical procedure

Twelve female Balb-C mice were used for calvarial defects. Mice were caged and handled in a sterile room at 22 °C and 50 % humidity with 12 hours of light and dark cycles. Before calvarial defect surgery, mice were under anesthesia via intraperitoneal injection using Zoletil and Rompun. Under anesthesia, incision was made on forehead, and 4-mm diameter of calvarial defect was performed using a hand drilling machine. Cryogels

were transplanted to defected sites, and mice were collected after ten weeks of transplantation.

Micro-computed tomography analysis

Defected sites of mice were collected and fixed with 4% paraformaldehyde solution. Images of surgical sites were obtained using Skyscan 1172 at 59 kV of operation source voltage, 167 μA of source current, and 40ms of an exposure time. Images obtained from micro-CT were evaluated via CT An.

Histological analysis

After fixing defected area and surrounding tissue of skulls in 4% paraformaldehyde solution for 24 hours, skulls were decalcified using 14% ethylenediaminetetraacetic acid (EDTA) at pH 7.4 for 4 days. Then, skulls were embedded in paraffin solutions and longitudinally sectioned at a thickness of 5 μm. Sectioned samples were deparaffinated using xylene solution, and gradually washed with tap water. Samples were stained with H&E staining and Masson's trichrome (MTC) staining and analyzed using light microscope (Olympus).

Statistical analysis

Quantitative data in this paper were presented in mean ± standard deviation. The statistical significance was determined using one-way analysis of variance (ANOVA) with $^{*}p < 0.05$, $^{**}p < 0.001$, and $^{***}p < 0.0001$.

2.3 Results

Synthesis of Methaycrylated Gelatin and Bioglass

Gelatin methacrylate was synthesized to provide crosslinking sites to conventional gelatin since gelatin requires a crosslinker like glutaraldehyde, which was reported as a cytotoxic material to permanently formed chemical crosslinking. Methacrylation of gelatin was studied using ^{1}H NMR. The characteristic peaks of acrylic hydrogen were present at 5.3 and 5.5 ppm, confirming the methacrylation of gelatin (Figure. 3).

Furthermore, bioglass nanoparticles (BGN) were prepared by sol-gel synthesis route. The size of bioglass was measured using scanning electron microscopy (SEM). Morphology of synthesized bioglass particles were rounded and amorphous, and were around 53.83±13.01 nm in size (Figure. 2). The Fourier-transform infrared spectroscopy (FT-IR) was used

to further analyze the structure of bioglass (Figure. 4). FT-IR spectrum showed characteristic bending vibration of phosphate group peaks at 561 and 603 cm^{-1}, and Si-O-Si stretching band at 1080 cm^{-1}.

After synthesizing BGN, bioactivity of BGN was tested if BGN possess biological effects after implantation. Bioactivity of BGN was confirmed via immersing BGN to simulated body fluid (SBF) solution for 14 days and compared with prepared BGN by X-ray powder diffraction (XRD). Hydroxyapatite peaks were presented in BGN soaked in SBF solution confirming the bioactivity of synthesized BGN (Figure. 4).

Characterization of bioglass embedded methacrylated gelatin cryogel

GelMA cryogels were synthesized via chemically crosslinking gelMA solution using ammonium persulfate and N, N, N', N'-tetramethylethylenediamine with desired concentration of BGN. The descending trend of swelling ratio was observed from 8.30 to 6.37 as bioglass was added to the cryogels. Furthermore, young's modulus of all groups were measured through analyzing stress vs strain graph. Expectedly, young's modulus of cryogel was increased as the concentration of BGN was increased from 84.67 ± 16.17 kPa to 178 ± 47.70 kPa (Figure. 5).

The degradation rates of cryogel were tested to observe whether

degradation rates of cryogels were dependent on the concentration of bioglass. The degradation time of cryogel was examined in the presence of collagenase II to measure the difference in degrading time due to bioglass concentration. Collagenase II was widely used to test degradation times of gelMA based cryogel [34, 35]. The degradation time was not significantly different from control group and experimental group due to relatively low concentration of BGN comparing to the concentration of gelMA (Figure. 6). Remaining mass percent after degrading 7 days of gelMA cryogel was 49.80 ± 2.91 % while remaining mass percents of cryogels for 0.5%, 1.5%, and 2.5% bioglass concentration were 66.33 ± 8.73 %, 60.48 ± 2.69%, and 64.02 ± 6.11 %.

Ion release rates were measured to observe the cumulative concentration of Si and Ca ions in the solution for particular days. The ion dissolution rates of BGN embedded GelMA cryogel in deionized water were gradually increased (Figure. 7).

Due to increase in young's modulus as the increase in concentration of bioglass incorporated to cryogel, internal structures of cryogels were observed to ensure that differences in porosity among experimental and control groups were negligible. The internal structures of BGN embedded gelMA cryogels were observed using SEM (Figure. 8). Since BGN was

physically mixed with gelMA solution when cryogel fabrication was performed, all experimental groups and the control group possessed similar internal structures.

Furthermore, cell permeabilities of scaffolds were examined via seeding GFP-tagged HELA cells on gelMA, and gelMA-bioglass cryogels, and observed using confocal after 24 hours (Figure. 8). Expectedly, all cryogel groups had uniform cell permeability abilities.

Hydroxyapatite formation in SBF solution

Various studies had confirmed the bioactivity of intact bioglass nanoparticle, yet bioactivities of cryogels which BGN was embedded were not emphasized. For measuring bioactivity of BGN embedded cryogels, they were incubated in SBF solution for 7 days, and phosphorus and silicon ion release kinetics were measured using inductively coupled plasma atomic emission spectrometer. Amounts of silicon ion release were increased while amounts of phosphorus ion release were decreased according to incubation time (Figure. 9). After seven days of incubation, internal structures of each group were observed through SEM for possible hydroxyapatite formation (Figure. 10). Furthermore, calcium to phosphate ratio on the surfaces of cryogels was calculated to be 1.63, which is very close to the literature value

of calcium to phosphorus ratio (Figure. 10).

Cell viability analysis

Cell viability tests were performed to investigate cytotoxicity of groups for further cellular responses. Observing fluorescence images of each group after incubating hTMSCs on cryogels for 24 hours, cell viabilities of each group were over 90% (Figure. 11).

Enhanced osteogenic responses on hTMSCs on gelMA-bioglass cryogel

After confirming hydroxyapatite formation and cytotoxicity, osteogenic potential of BGN embedded cryogels were confirmed via seeding human tonsil-derived mesenchymal stem cells (hTMSCs) on the top of cryogels, and cultured with osteogenic medium for 7 and 14 days for measuring relative osteogenic gene expression. Both on day 7 and day 14, quantitative real-time PCR analysis of osteogenic markers such as osteocalcin, collagen I, and runt-related transcription factor 2 confirmed that hTMSCs seeded on cryogels with higher concentration of bioglass (1.5% and 2.5% of BGN) expressed higher bone-related gene expressions, including 7.84 (1.5% BGN) and 13.13 (2.5% BGN) fold increase in OCN, 13.56 (1.5% BGN) and 29.92 (2.5% BGN) fold increase in Col I, and 6.47

(1.5% BGN) and 12.83 (2.5% BGN) fold increase in Runx2 compare to gelMA cryogel at day 14 (Figure. 12). However, relative gene expression of gelMA cryogel and gelMA-0.5% bioglass cryogel were not highly significant on day 7 and day.

Further investigating cellular responses of hTMSCs, hTMSCs were cultured on dish in osteogenic medium with similar concentration of bioglass for 21 days. Then, the amounts of calcium deposition of each sample were measured using alizarin red staining (Figure. 13). The result was similar with that of quantitative real-time PCR since higher calcium contents were observed as dosages of bioglass were increased.

In vivo bone regeneration after implanting bioglass embedded gelMA cryogel

To validate the optimal concentration of BGN embedded in gelMA cryogels for effective bone regeneration, in vivo studies were conducted. GelMA-bioglass cryogels were implanted to calvarial defect areas of balb/c mice. Then, bone regenerations of defected areas were evaluated using micro-CT after eight weeks from transplantation (Figure. 14). Similar to *in vitro* cell studies, BV/TV of cryogels containing the highest bioglass concentration had 3.89 fold higher comparing to control group.

In addition, cell penetration on scaffold was evaluated via histology. Histological analysis of H&E staining and Masson's trichrome staining (MTC) showed that as the concentration of bioglass increased, higher collagen was found inside the transplanted cryogels (Figure. 15). Histological analysis and micro-CT confirmed that gelMA-2.5% bioglass cryogel showed the highest enhancement in bone regeneration comparing to other experimental group.

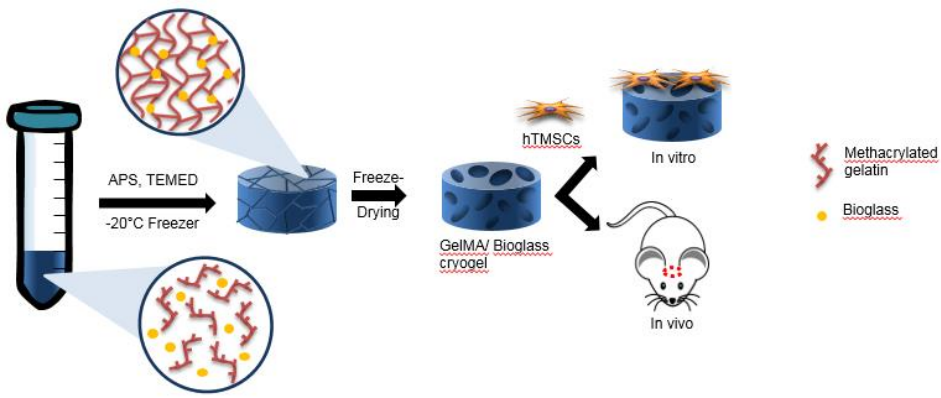

Figure 1. Overall schematic figure of the experiment with human tonsil derived mesenchymal stem cells and gelMA-bioglass cryogel

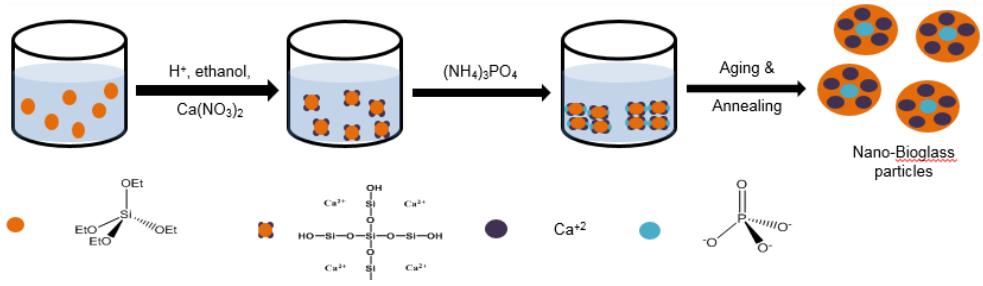

Figure 2. Schematic figure of the synthesizing bioglass nanoparticle

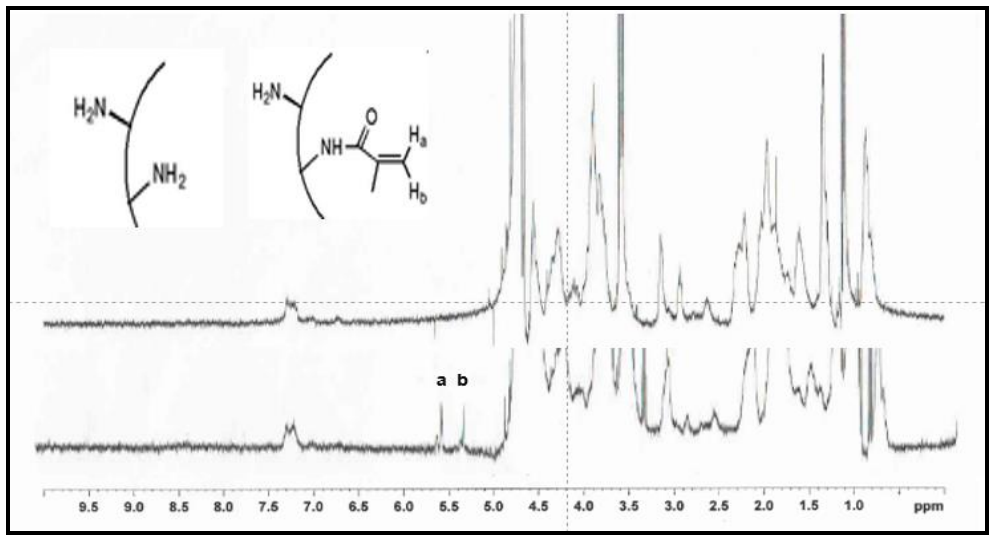

Figure 3. ^{1}H NMR of gelatin and methacrylated gelatin

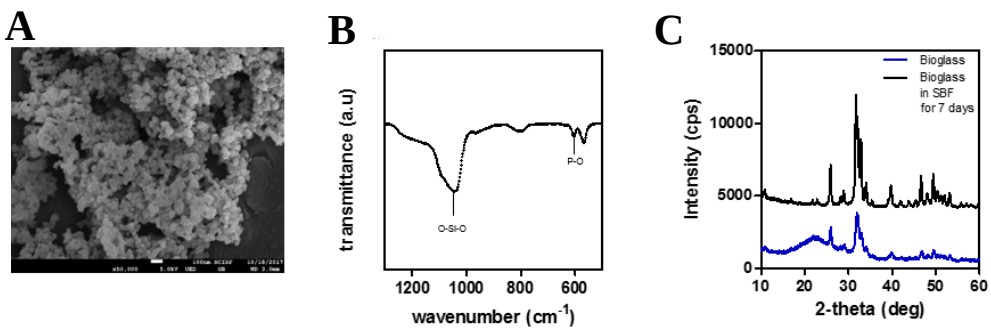

Figure 4. Bioglass characterization. (A) SEM image of bioglass nanoparticles, (B) FTIR spectrum of bioglass nanoparticle, (C) XRD spectrum of bioglass and bioglass soaking in simulated body fluid solution for 7 days

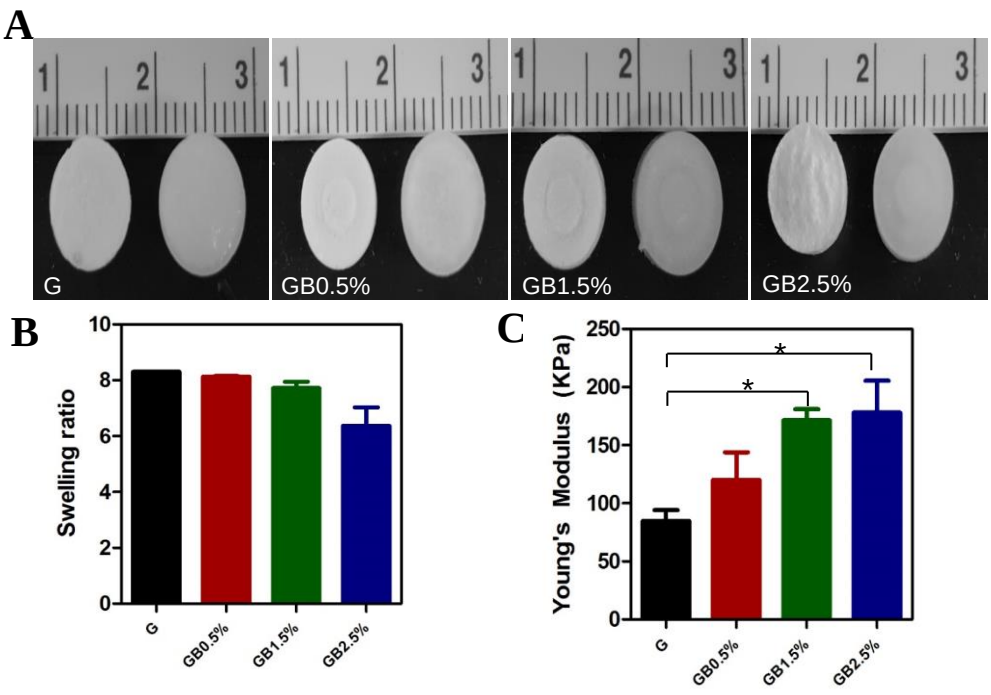

Figure 5. Bioglass incorporated gelMA cryogel characterization. (A) Gross image of dried and swollen cryogels. (B) Swelling ratio of each experimental group (n=3) after swelling in DPBS for 24 hours: **p*-value<0.05. (C) Young's modulus for each cryogels (n=3): **p*-value<0.05

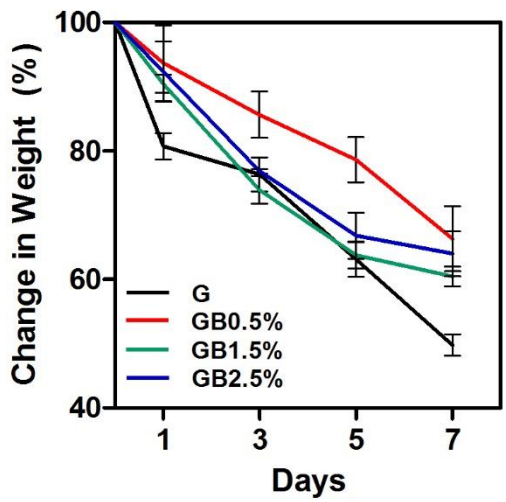

Figure 6. Degradation of rates of each cryogel (n = 3)

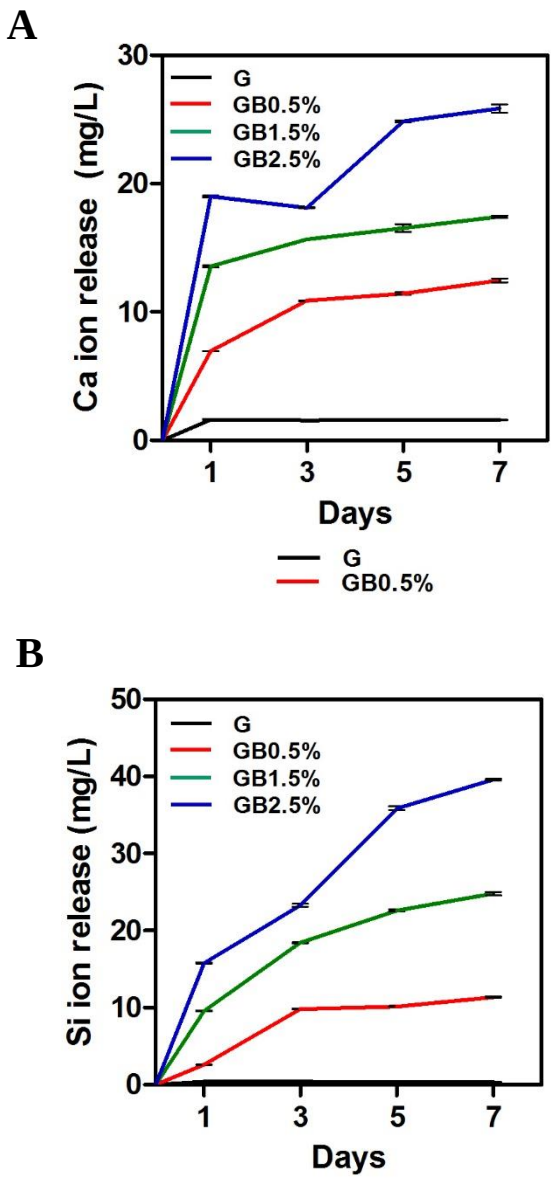

Figure 7. Ion release rates of (A) Ca and (B) Si ion from each cryogel in deionized water for 7 days

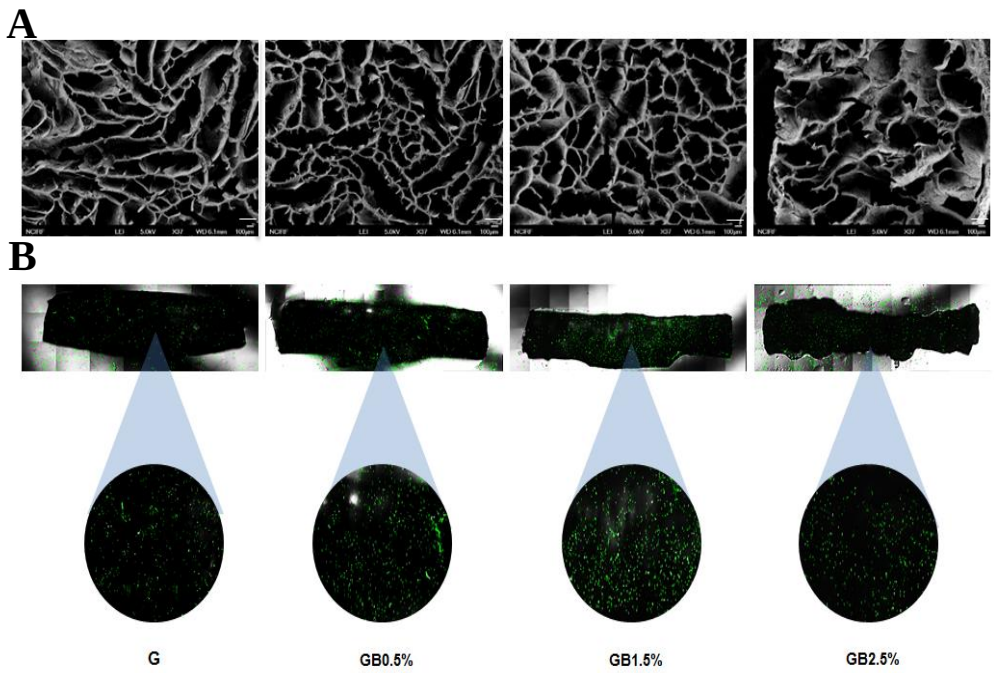

Figure 8. (A) SEM images of each cryogels at x32 and (B) Confocal images of cryogels for confirming cell permeability

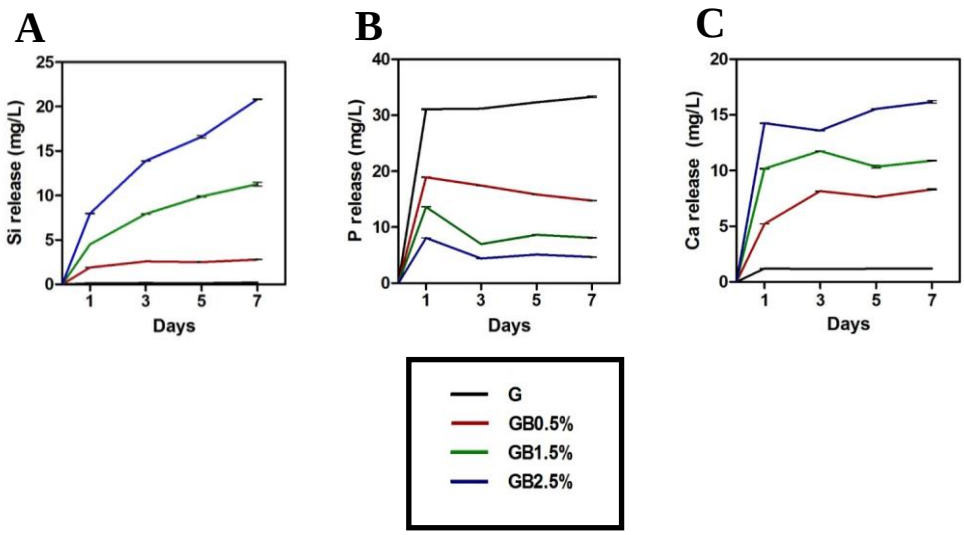

Figure 9. releasing rates of (A) Si, (B) P, (C) Ca ion from cryogels in simulated body fluid solution for 7 days (n=3)

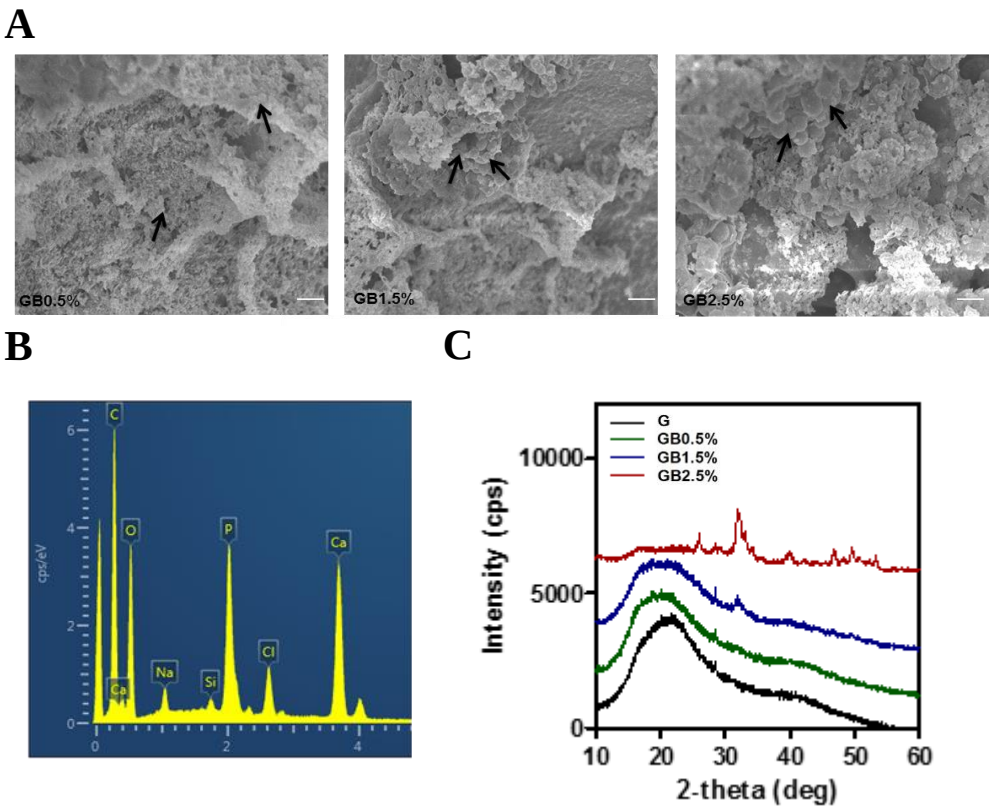

Figure 10. Bioactivities of cryogels (A) SEM images of cryogels after soaking in SBF solution in 7 days (B) EDS mapping on the surface of 2.5 % bioglass embedded cryogel (C) XRD spectrum of cryogels after soaking in SBF solution for 7 days (n=3)

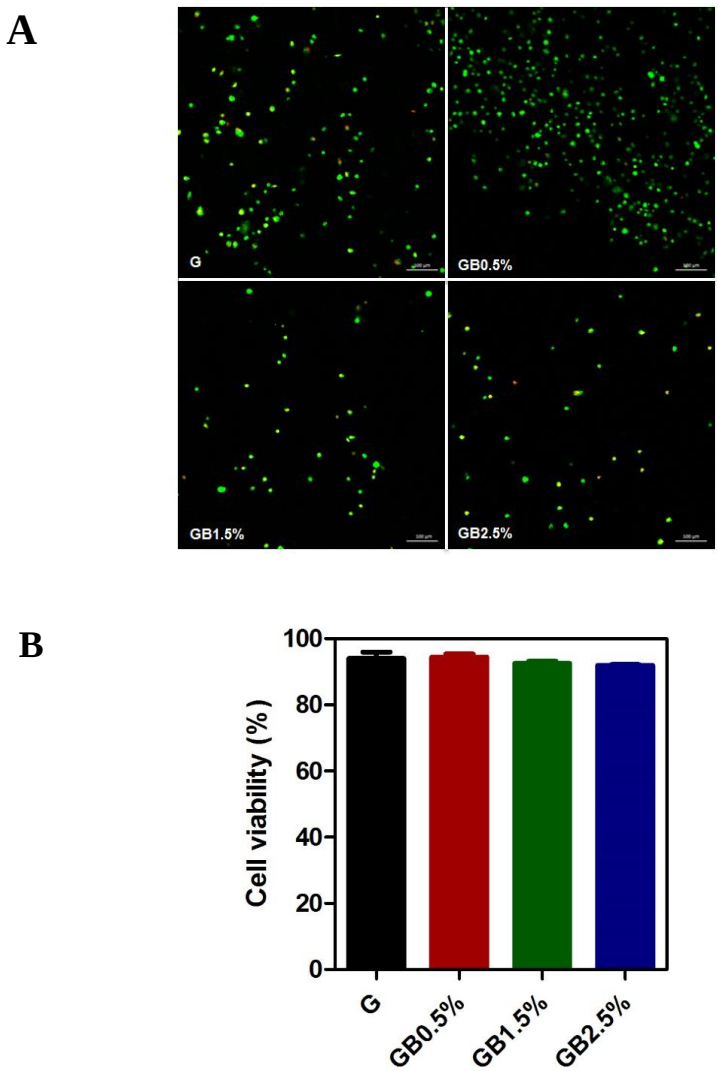

Figure 11. Cell viability analysis (a) Live/dead viability images of each experimental group. Live cells were stained with Calcein AM (green) and dead cells were stained with ethidium homodimer-1 (red). Scale bar = 100μm (b) Cell viability of each cryogels (n = 3) was quantified via calculating the ratio between live cells and dead cells

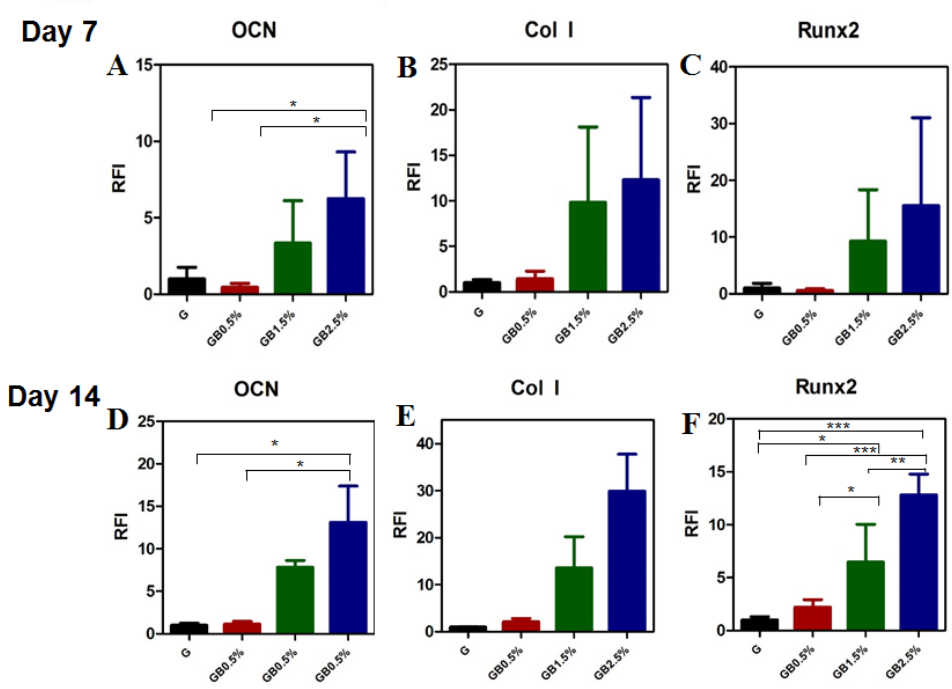

Figure 12. Osteogenic differentiation of human tonsil-derived mesenchymal stem cells (hTMSCs). Relative gene expression of OCN, Col I, and Runx2 at day 7 (A~C), and day 14(D~F):*p-value<0.05, **p-value<0.001 ***p-value<0.0001.

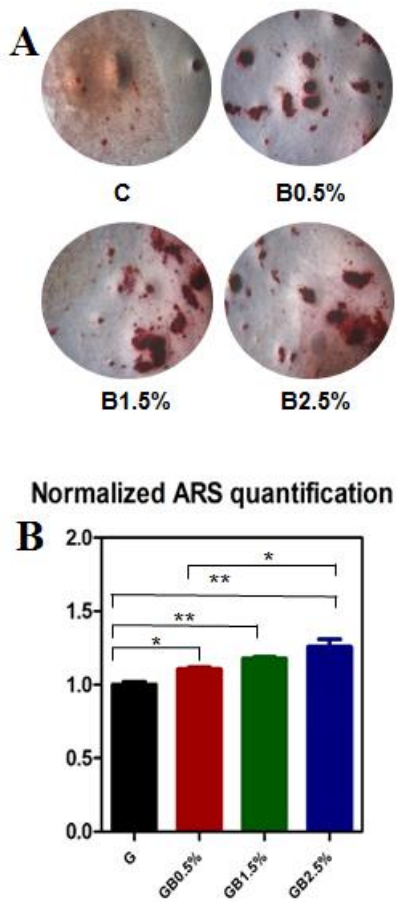

Figure 13. Alizarin red staining. (A) Alizarin red staining images of hTMSCs after culturing in osteogenic media for 21 days. (B) Quantitative analysis of alizarin red staining:*p-value<0.05, **p-value<0.001 ***p-value<0.0001.

A

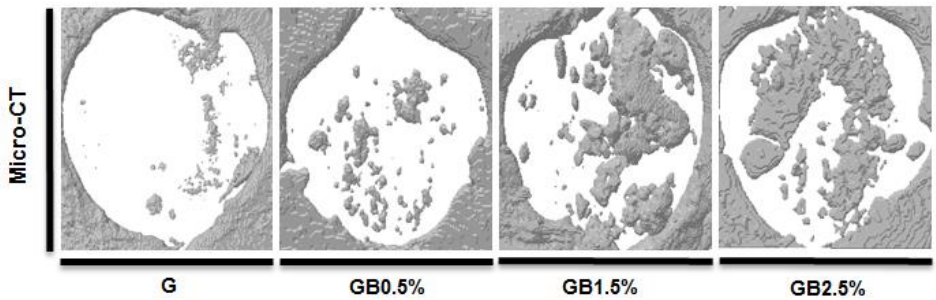

B

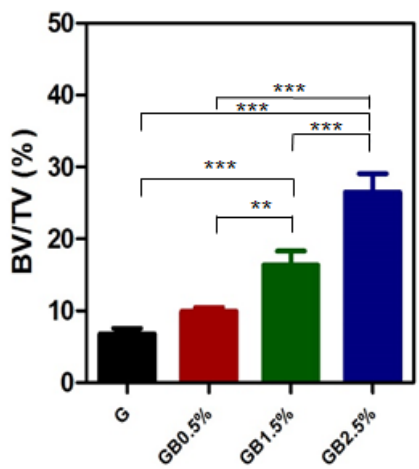

Figure 14. Osteogenic effect of bioglass after implantation. (A) Micro-CT image of bone defects on each group (n = 3), and (B) the ratio of bone volume and total volume: **p*-value<0.05, ***p*-value<0.001, ****p*-value<0.0001

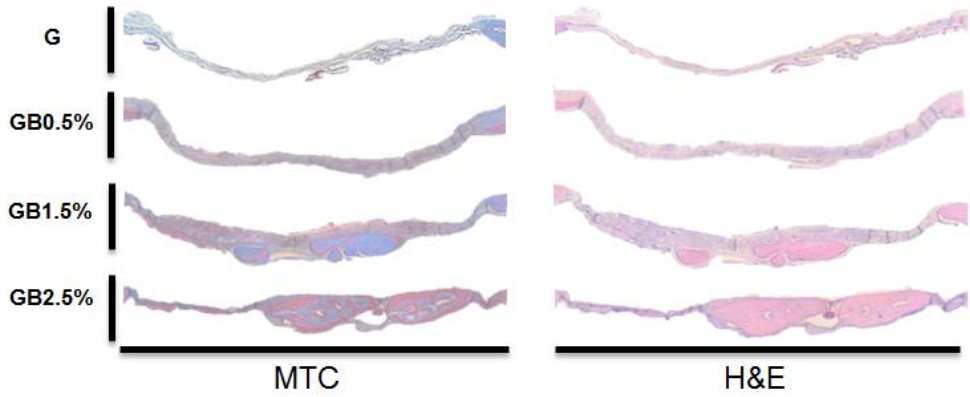

Figure 15. Histological analysis of MTC and H&E

2.4 Discussion

Implanting synthetic calcium phosphate-based materials are widely studied for regenerating defected bone area. Bioglass is an inorganic mineral, which enhances osteogenic differentiation via releasing osteoinductive ions, and forming hydroxyapatite. Various studies demonstrate the effects of ions on bone regeneration process [36-40]. In addition to supplying calcium phosphate, providing extracellular matrix-like environment enhances bone regeneration during bone healing process [41, 42]. Due to mimicking natural extracellular matrix (ECM) and having porous structure, cryogels were widely used in tissue engineering [43, 44]. From this idea, we embedded bioglass into gelMA cryogels to provide not only osteoinducing ions, but also natural extracellular matrix. We hypothesized that bioglass embedded within macroporous GelMA based cryogel would provide osteogenic-friendly environment. Furthermore, macroporous structure of GelMA would provide cancellous bone-like structure, where host stem cells can migrate. Closer look at the microcture of GelMA based cryogel showed that the overall pore size was independent of bioglass addition. However, physical adhesion between GelMA and bioglass may have contributed to the bioglass concentration dependent reduction in swelling

ratio and increase in mechanical properties of cryogel. Previously, Pluharova et al. has demonstrated that ion-dipole interaction persists between amide group and calcium ions [45]. Thus, this physical adhesion in combination with ion-dipole interactions from calcium ions dissoluted from bioglass and amide group in GelMA may have contributed overall physical characterics of crygels.

Mineralization of inorganic minerals plays an important role in maintaining bioactivities in body fluids [46, 47]. The mechanism of surface chemistry and bioactivity on bioglass powder in SBF solution was widely studied [48, 49]. However, bioactivity of bioglass in a cryogel was not further explored. From the result obtained via testing bioactivities of bioglass embedded cryogels, the formation of hydroxyapatite was observed via XRD. However, the ion concentration thresholds seemed to be present according to XRD. The amount of mineral deposited was gradually increased with the concentration of bioglass until 1.5% and sharp increase with 2.5% bioglass concentration (Figure. 10). This result suggests that the minimum amount of bioglass is required to trigger hydroxyapatite formation in early periods since rate of hydroxyapatite formation is depended on presence of Ca and P ions. This result is similar from the findings of Hench et al when authors found the rate of hydroxyapatite formation is depended

on concentration of bioglass [50].

Ion release rates of Si, Ca, P ions from bioglass immersing in SBF solution reveal that Si ions were released to form silanol and enhancing overall hydroxyapatite formation via forming apatite nuclei (Figure. 9). After forming apatite nuclei, the saturation of Ca ions reached in the solution. Then, the hydroxyapatite layer was formed via recapturing and adsorbed P ions, which were released to the solution on the apatite nuclei. Thus, the concentrations of P ion were decreased as the time passed.

Furthermore, the mineralized surfaces of cryogels were measured via EDS mapping, and the only gelMA-2.5% bioglass group showed apatite with 1.63 Ca/P ratio, which was similar to theoretical Ca/P value of 1.67 (Figure. 10). This result suggests a possible direct cryogel-bone bonding, which may increase the *in vivo* bone generation [51].

Osteogenic effects of bioglass embedded GelMA cryogels on hTMSCs were measured using RT-PCR and alizarin red staining. In our studies, Osteogenic genes (OCN, Runx2, and Col I) were further upregulated according to the concentration of bioglass on day 7 and day 14 (Figure. 12), and the similar trend was observed when calcium deposition was measured after 21 days via alizarin red staining (Figure. 13). Osteogenic differentiation of hTMSCs was enhanced due to ion dissolutions

from bioglass in osteogenic medium since similar trend of Ca and Si ion release rates were observed according to bioglass dosage embedded in cryogel (Figure. 7 and Figure. 12). Calcium ion released from bioglass enhanced mineralization, inducing guiding stem cells to osteoblasts [52]. Furthermore, S. Maeno et al. further supports that Ca ion induces osteogenic differentiation in both monolayer and 3D culture [53]. Our study confirmed that osteogenic differentiation of hTMSCs were dependent on the concentration of bioglass incorporated in cryogel. Si ion, an ion composing bioglass, is well-known ion that induces bone formation and calcification in the early stage, yet, high concentration of Si ion increases cytotoxicity. In our studies, the concentration of silicon ion in bioglass was minimal so cells seeded on cryogel with the highest concentration of bioglass exhibited similar cytotoxicity to cells seed on control group (Figure. 11).

Based on *in vitro* results, cryogels were implanted for 8 weeks and measured improved bone regeneration in a calvarial defect. Similar to *in vitro* results, bioglass helps bone regeneration of defected area. Analyzing with micro-CT, cryogels with the highest concentration of bioglass had the most bone healing compared to other cryogel groups (Figure. 14). Furthermore, higher concentration of collagen was observed via Masson's trichrome staining and H&E staining in the highest bioglass concentration

group. Conclusively, bioglass has an osteoinducing effect in bone healing process.

CONCLUSION

From our study, bioglass embedded cryogel not only induced osteogenic differentiation of hTMSCs, but also was bioactive via forming hydroxyapatite on its surface. Thus, by maximizing dose-dependency of bioglass and its cytotoxicity, bioglass incorporated cryogel will be a potential candidate in clinical application for bone tissue engineering.

REFERENCE

1. Fillingham, Y. and J. Jacobs, *Bone grafts and their substitutes.* Bone Joint J, 2016. **98-B**(1 Suppl A): p. 6-9.
2. Hofbauer, M.H., R.J. Delmonte, and M.L. Scripps, *Autogenous bone grafting.* J Foot Ankle Surg, 1996. **35**(5): p. 386-90.
3. Giannoudis, P.V., et al., *Masquelet technique for the treatment of bone defects: tips-tricks and future directions.* Injury, 2011. **42**(6): p. 591-8.
4. Cox, G., et al., *Reamer-irrigator-aspirator indications and clinical results: a systematic review.* Int Orthop, 2011. **35**(7): p. 951-6.
5. Huffman, L.K., J.G. Harris, and M. Suk, *Using the bi-masquelet technique and reamer-irrigator-aspirator for post-traumatic foot reconstruction.* Foot Ankle Int, 2009. **30**(9): p. 895-9.
6. Jones, J.R. and L.L. Hench, *Materials perspective - Biomedical materials for new millennium: perspective on the future.* Materials Science and Technology, 2001. **17**(8): p. 891-900.
7. Betz, R.R., *Limitations of autograft and allograft: new synthetic solutions.* Orthopedics, 2002. **25**(5 Suppl): p. s561-70.
8. Pina, S., J.M. Oliveira, and R.L. Reis, *Natural-based nanocomposites for bone tissue engineering and regenerative medicine: a review.* Adv Mater, 2015. **27**(7): p. 1143-69.
9. Venkatesan, J., et al., *Alginate composites for bone tissue engineering: a review.* Int J Biol Macromol, 2015. **72**: p. 269-81.
10. Cox, S.C., et al., *3D printing of porous hydroxyapatite scaffolds intended for use in bone tissue engineering applications.* Mater Sci Eng C Mater Biol Appl, 2015. **47**: p. 237-47.
11. Bose, S., M. Roy, and A. Bandyopadhyay, *Recent advances in bone tissue engineering scaffolds.* Trends Biotechnol, 2012. **30**(10): p. 546-54.
12. Chen, Q.Z., I.D. Thompson, and A.R. Boccaccini, *45S5 Bioglass-derived glass-ceramic scaffolds for bone tissue engineering.* Biomaterials, 2006. **27**(11): p. 2414-25.
13. Savina, I.N., I.Y. Galaev, and B. Mattiasson, *Ion-exchange macroporous*

hydrophilic gel monolith with grafted polymer brushes. J Mol Recognit, 2006. **19**(4): p. 313-21.

14. Baker, M.I., et al., *A review of polyvinyl alcohol and its uses in cartilage and orthopedic applications.* J Biomed Mater Res B Appl Biomater, 2012. **100**(5): p. 1451-7.
15. Petrenko, Y.A., et al., *Comparison of the methods for seeding human bone marrow mesenchymal stem cells to macroporous alginate cryogel carriers.* Bull Exp Biol Med, 2011. **150**(4): p. 543-6.
16. Rahman, C.V., et al., *PLGA/PEG-hydrogel composite scaffolds with controllable mechanical properties.* J Biomed Mater Res B Appl Biomater, 2013. **101**(4): p. 648-55.
17. Hahn, M.S., et al., *Photolithographic patterning of polyethylene glycol hydrogels.* Biomaterials, 2006. **27**(12): p. 2519-24.
18. Yamamoto, M., Y. Ikada, and Y. Tabata, *Controlled release of growth factors based on biodegradation of gelatin hydrogel.* J Biomater Sci Polym Ed, 2001. **12**(1): p. 77-88.
19. Wu, S., et al., *Biocompatible chitin/carbon nanotubes composite hydrogels as neuronal growth substrates.* Carbohydr Polym, 2017. **174**: p. 830-840.
20. Koshy, S.T., et al., *Injectable, porous, and cell-responsive gelatin cryogels.* Biomaterials, 2014. **35**(8): p. 2477-87.
21. Davidenko, N., et al., *Evaluation of cell binding to collagen and gelatin: a study of the effect of 2D and 3D architecture and surface chemistry.* J Mater Sci Mater Med, 2016. **27**(10): p. 148.
22. Mazaki, T., et al., *A novel, visible light-induced, rapidly cross-linkable gelatin scaffold for osteochondral tissue engineering.* Sci Rep, 2014. **4**: p. 4457.
23. Son, T.I., et al., *Visible light-induced crosslinkable gelatin.* Acta Biomater, 2010. **6**(10): p. 4005-10.
24. Han, M.E., et al., *Gelatin-based extracellular matrix cryogels for cartilage tissue engineering.* Journal of Industrial and Engineering Chemistry,

2017. **45**: p. 421-429.

25. Chen, Y.C., et al., *Functional Human Vascular Network Generated in Photocrosslinkable Gelatin Methacrylate Hydrogels.* Adv Funct Mater, 2012. **22**(10): p. 2027-2039.
26. Zuo, Y., et al., *Photo-cross-linkable methacrylated gelatin and hydroxyapatite hybrid hydrogel for modularly engineering biomimetic osteon.* ACS Appl Mater Interfaces, 2015. **7**(19): p. 10386-94.
27. Rahaman, M.N., et al., *Bioactive glass in tissue engineering.* Acta Biomater, 2011. **7**(6): p. 2355-73.
28. Gerhardt, L.C. and A.R. Boccaccini, *Bioactive Glass and Glass-Ceramic Scaffolds for Bone Tissue Engineering.* Materials (Basel), 2010. **3**(7): p. 3867-3910.
29. Ros-Tarraga, P., et al., *Assessment of Effects of Si-Ca-P Biphasic Ceramic on the Osteogenic Differentiation of a Population of Multipotent Adult Human Stem Cells.* Materials (Basel), 2016. **9**(12).
30. Barradas, A.M., et al., *A calcium-induced signaling cascade leading to osteogenic differentiation of human bone marrow-derived mesenchymal stromal cells.* Biomaterials, 2012. **33**(11): p. 3205-15.
31. Kendrick, J. and M. Chonchol, *The role of phosphorus in the development and progression of vascular calcification.* Am J Kidney Dis, 2011. **58**(5): p. 826-34.
32. Lin, F.H., et al., *The bonding behavior of DP-Bioglass and bone tissue.* Materials Chemistry and Physics, 1996. **46**(1): p. 36-42.
33. Gomez-Vega, J.M., et al., *Bioactive glass coatings with hydroxyapatite and Bioglass particles on Ti-based implants. 1. Processing.* Biomaterials, 2000. **21**(2): p. 105-11.
34. Hutson, C.B., et al., *Synthesis and characterization of tunable poly(ethylene glycol): gelatin methacrylate composite hydrogels.* Tissue Eng Part A, 2011. **17**(13-14): p. 1713-23.
35. Benton, J.A., et al., *Photocrosslinking of gelatin macromers to synthesize porous hydrogels that promote valvular interstitial cell function.* Tissue

Eng Part A, 2009. **15**(11): p. 3221-30.

36. Hanawa, T., et al., *Early bone formation around calcium-ion-implanted titanium inserted into rat tibia.* J Biomed Mater Res, 1997. **36**(1): p. 131-6.
37. Maeda, H., T. Kasuga, and L.L. Hench, *Preparation of poly(L-lactic acid)-polysiloxane-calcium carbonate hybrid membranes for guided bone regeneration.* Biomaterials, 2006. **27**(8): p. 1216-22.
38. Khan, A.F., et al., *Bioactive behavior of silicon substituted calcium phosphate based bioceramics for bone regeneration.* Mater Sci Eng C Mater Biol Appl, 2014. **35**: p. 245-52.
39. Shie, M.Y., S.J. Ding, and H.C. Chang, *The role of silicon in osteoblast-like cell proliferation and apoptosis.* Acta Biomater, 2011. **7**(6): p. 2604-14.
40. Boonrungsiman, S., et al., *The role of intracellular calcium phosphate in osteoblast-mediated bone apatite formation.* Proc Natl Acad Sci U S A, 2012. **109**(35): p. 14170-5.
41. Shekaran, A. and A.J. Garcia, *Extracellular matrix-mimetic adhesive biomaterials for bone repair.* J Biomed Mater Res A, 2011. **96**(1): p. 261-72.
42. Mansour, A., et al., *Extracellular Matrices for Bone Regeneration: A Literature Review.* Tissue Eng Part A, 2017.
43. Hixon, K.R., et al., *The calcification potential of cryogel scaffolds incorporated with various forms of hydroxyapatite for bone regeneration.* Biomed Mater, 2017. **12**(2): p. 025005.
44. Kim, H.D., et al., *Biomimetic whitlockite inorganic nanoparticles-mediated in situ remodeling and rapid bone regeneration.* Biomaterials, 2017. **112**: p. 31-43.
45. Pluharova, E., et al., *Aqueous Cation-Amide Binding: Free Energies and IR Spectral Signatures by Ab Initio Molecular Dynamics.* J Phys Chem Lett, 2014. **5**(13): p. 2235-40.
46. Wu, C., et al., *A novel bioactive porous bredigite (Ca7MgSi4O16) scaffold with biomimetic apatite layer for bone tissue engineering.* J

Mater Sci Mater Med, 2007. **18**(5): p. 857-64.

47. Ghomi, H., M.H. Fathi, and H. Edris, *Effect of the composition of hydroxyapatite/bioactive glass nanocomposite foams on their bioactivity and mechanical properties.* Materials Research Bulletin, 2012. **47**(11): p. 3523-3532.
48. Hench, L.L., *Bioceramics - from Concept to Clinic.* Journal of the American Ceramic Society, 1991. **74**(7): p. 1487-1510.
49. Filgueiras, M.R., G. La Torre, and L.L. Hench, *Solution effects on the surface reactions of a bioactive glass.* J Biomed Mater Res, 1993. **27**(4): p. 445-53.
50. Jones, J.R., P. Sepulveda, and L.L. Hench, *Dose-dependent behavior of bioactive glass dissolution.* J Biomed Mater Res, 2001. **58**(6): p. 720-6.
51. Rezwan, K., et al., *Biodegradable and bioactive porous polymer/inorganic composite scaffolds for bone tissue engineering.* Biomaterials, 2006. **27**(18): p. 3413-31.
52. Nakamura, S., et al., *Effect of calcium ion concentrations on osteogenic differentiation and hematopoietic stem cell niche-related protein expression in osteoblasts.* Tissue Eng Part A, 2010. **16**(8): p. 2467-73.
53. Maeno, S., et al., *The effect of calcium ion concentration on osteoblast viability, proliferation and differentiation in monolayer and 3D culture.* Biomaterials, 2005. **26**(23): p. 4847-55.

요약(국민초록)

바이오글라스 기반 생체재료를 통한 줄기세포의 골형성 유발

현재까지 골 재생을 유도하기 위하여 다양한 방법의 연구가 진행되어왔다. 그 중, 조직공학은 줄기세포와 생체모방 생체재료를 이용한 재생치료에 중점을 두고 있다. 이 연구에서 사용되는 젤라틴은 콜라젠에서부터 얻어낸 물질로써 인체에 무해한 물질로 조직 공학에서 골재생뿐 아니라 다양한 용도로 사용되어 왔다. 또한, 골 재생 과정에서 인산과 칼슘 이온이 줄기세포의 골분화를 유도하기 위하여 자주 사용되어 왔다. 이번 연구의 목적은 골 재생을 위하여 인삼칼슘이 주 성분인 바이오글라스의 농도에 따른 인간편도유래 중간엽 줄기세포의 골 분화 효과를 보는 것이었다. 이번 연구는 골 재생이 다양한 농도의 바이오글라스 기반 생체재료에 따른 인간편도유래 중간엽 줄기세포의 골 분화 향상을 보여주었다.

주요어: 바이오글라스, 메타크릴레이트 젤라틴, 크라이오젤, 골분화

학번: 2015-22824